Electronic Supplementary Information

Design of Photoelectrochemical Device for the Selective Conversion of Aqueous CO_2 to CO: Using Mesoporous Paladium-Copper Bimetallic Cathode and Hierarchical ZnO-based Nanowire Arrays Photoanode

Mu Li,[ab] Peng Li,[a*] Kun Chang,[a] Huimin Liu,[a] Xiao Hai,[ab] Huabin Zhang[a] and Jinhua Ye[abcd*]

[a]Photocatalytic Materials Group, National Institute for Materials Science 1-1 Namiki, Tsukuba, Ibaraki 305-0044 (Japan) E-mail: Jinhua.YE@nims.go.jp; Li.Peng@nims.go.jp

[b]Graduate School of Chemical Science and Engineering, Hokkaido University, Sapporo 060-0814 (Japan)

[c]TU-NIMS Joint Research Center, School of Material Science and, Engineering, Tianjin University, 92 Weijin Road, Tianjin (P.R. China)

[d]Collaborative Innovation Center of Chemical Science and Engineering (Tianjin), Tianjin 300072, P. R. China.

Experimental

Preparation of mesoporous Pd-Cu electrocatalysts. The detailed preparation process was shown in our previous report. Briefly, to fabricate mesoporous Pd-Cu electrodes, a constant potential was carried out at -0.2 V by using an electrochemical machine (CHI 660D electrochemical analyzer, CH Instrument, U.S.) with a standard three-electrode cell system, including an Ag/AgCl (saturated KCl) electrode as a reference electrode, a platinum wire as a counter electrode. Glassy Carbon (GC) substrate was employed as the working electrode for the measurements of electrocatalytic

of CO_2, while ITO substrate was used as working electrode for sample characterizations. The electrolyte solution used contained $PdCl_2$ and $Cu(NO_3)_2$ with Brij 58 ($C_{16}H_{33}(OCH_2CH_2)_{20}OH$, 1.0 wt%) as the surfactant. $PdCl_2$ and $Cu(NO_3)_2{\cdot}3H_2O$ were used as the metal sources. The total concentration of metal precursors was 10 mM. The molar ratios of Pd to Cu species were gradually changed (Pd^{2+}/Cu^{2+} =10:0, 7:3, 5:5, 3:7 and 0:10, respectively) for the preparation of mesoporous Pd-Cu electrodes with different compositions. After electrodeposition for 600 s, as-prepared films were soaked in ethanol for 24 h to extract the surfactants, then thoroughly rinsed with de-ionized water, and dried in air. Nanoparticle Pd_7Cu_3 was prepared as the same method without Brij 58 surfactant. Nanoparticle Pd_7Cu_3 and mesoporous Pd_7Cu_3 were abbreviated as N-PdCu and M- PdCu, respectively.

Fabrication of pristine ZnO NWs and ternary CNTs-ZnO-Co_3O_4 NWs composite photoanodes. ZnO NWs were prepared by a facile hydrothermal synthesis process. Briefly, 100 mL of a 0.06 M solution of zinc acetate in absolute ethanol was prepared with ultrasonic agitation as seeds solution. The seeds solution was spin-coated on the pre-treated FTO substrates, and then annealed at 350 °C for 30 min to yield a layer of ZnO seeds. The seeded substrates were suspended vertically in a Teflon vessel, and then sealed in an autoclave and heated to 110 °C for

24 h for nanowire growth. The reagent solution was 0.06 M zinc nitrate and 0.06 M hexamethylenetetramine (HMT) aqueous solution. Finally, the nanowire substrate was removed from the autoclave, washed thoroughly with distilled water, dried in air and annealed at 300 °C for 3h in air. Then CNTs-ZnO NWs were obtained by soaking the as-prepared ZnO NWs in CNTs aqueous solution (concentration of 0.25 mg mL^{-1},). CNTs powders (Multi-walled, 40~70 nm, Wako) were treated with 3:1 H_2SO_4/HNO_3 mixture for functionalization and better dispersion in water before use. The ZnO/FTO substrates were immersed in the CNTs aqueous solution for 30s, died in air and annealed at 300 °C for 3h in air. The as-obtained CNTs-ZnO/FTO substrates were subsequently used as the working electrode and placed in an electrochemical cell which was assembled in a three-electrode configuration, by using platinum as the counter electrode and Ag/AgCl as the reference electrode. The electrodeposition of cobalt precursors were carried out by galvanostatic deposition at a current density of 1 mA cm^{-2} in 0.15 M $Co(NO_3)_2$ aqueous solution. Finally, the resulting nanowire arrays were withdrawn, rinsed with distilled water and annealed at 300 °C for 3h in air. Pristine ZnO NWs and ternary CNTs-ZnO-Co_3O_4 NWs composite were abbreviated as P-ZnO and T-ZnO, respectively.

Characterization Scanning electron microscopy (SEM) was conducted with a HITACHI S-4800 field emission scanning electron microscopy. Transmission electron microscopy (TEM) and High-resolution TEM (HRTEM) images were recorded with a field emission transmission electron microscope (2100F, JEOL Co., Japan) operated at 200 kV, combined with energy dispersive X-ray spectroscopy (EDX) for the determination of metal composition. X-ray diffraction (XRD) patterns were recorded on an Intelligent XRD system (SmartLab, Rigaku Corporation, Japan). X-ray Photoelectron Spectroscopy (XPS) experiments were performed in type Theta probe (ULVAC-PHI, Japan) using monochromatized Al Kα at 1.4×0.1 mm 100 W(20 kV, 5 mA) and the peak positions were internally referenced to the C 1s peak at 285.0 eV.

Electrochemical measurements. The electrocatalytic reduction of CO_2 was measured on a CHI 660D electrochemical workstation in aqueous 0.1 M $KHCO_3$ solution (pH ≈ 6.8). The electrolyte solution was purged by Ar gas and saturated with CO_2 successively before the measurement. The experiments were performed in a gas-tight two compartment H-cell separated by a Nafion117 film. Platinum and Ag/AgCl (in saturated KCl) electrode were selected as the counter electrode and reference electrode, respectively. All of the applied potentials were recorded against Ag/AgCl (saturated KCl) reference electrode and then converted to reversible hydrogen electrode (RHE). The products of reduction half reactions in cathodic side were sampled and measured with a gas chromatograph (GC). The main products of CO_2 reduction CO and other carbon products were sampled and measured with a gas chromatograph (GC-14B, Shimadzu) equipped with a flame ionization detector (FID) according to the standard curves. The GC column is Porapak Q-methanizer for CO and CO_2 measurement, PEG1000 for organic products measurement. The product of competing water reduction reaction H_2 was measured with a gas chromatograph (GC-8A, Shimadzu) with a TCD detector according to the standard curve. The GC column is 5A molecular sieve.

Photoelectrochemical measurements. The overall photoelectrochemical (PEC) conversion of CO_2 was measured on a CHI 660D electrochemical workstation. The electrolyte solution was aqueous 0.1 M $KHCO_3$ solution at cathodic side and 0.1 M K_2SO_4 at the anodic side in a gas-tight two compartment H-cell separated by a Nafion117 film. Both of the solutions were purged by Ar gas and the cathodic side was saturated with CO_2 successively before the measurement. The phorocurrent response was investigated under the illumination of an AM 1.5 solar simulator (WXS-80C-3 AM 1.5G, 100 mW cm^{-2}) in a two-electrode cell system, with mesoporous Pd_7Cu_3 alloy electrocatalysts (0.07 cm^2) as cathode and hierarchical CNTs-ZnO-Co_3O_4 NWs composite as photoanode (1 cm^2). Nanoparticle Pd_7Cu_3 alloy (N-PdCu) which was prepared without Brij

58 surfactant was also performed as cathode and pristine ZnO NWs (P-ZnO) as well as Pt foil was also used as anode to contrast with the designed mesoporous Pd_7Cu_3 alloy (M-PdCu) cathode and the ternary CNTs-ZnO-Co_3O_4 NWs composite (T-ZnO) photoanode PEC device. The products of reduction half reactions in cathodic side were sampled and measured with a gas chromatograph (GC). The main products of CO_2 reduction CO and other carbon products were sampled and measured with a gas chromatograph (GC-14B, Shimadzu) equipped with a flame ionization detector (FID) according to the standard curves. The GC column is Porapak Q-methanizer for CO and CO_2 measurement, PEG1000 for organic products measurement. The product of competing water reduction reaction H_2 was measured with a gas chromatograph (GC-8A, Shimadzu) with a TCD detector according to the standard curve. The GC column is 5A molecular sieve. The incident photon to electron conversion efficiency (IPCE) was calculated from chronoamperometry measurements using a motorized monochrometer (M10; Jasco Corp.). IPCE can be expressed as IPCE = 1240 $j_p(\lambda)$ / $\lambda E_\lambda(\lambda)$, where $j_p(\lambda)$ is the measured photocurrent density (mA cm^{-2}), λ is the incident light wavelength (nm) and $E_\lambda(\lambda)$ is the incident monochromatic light power density (mW cm^{-2}) at a specific wavelength

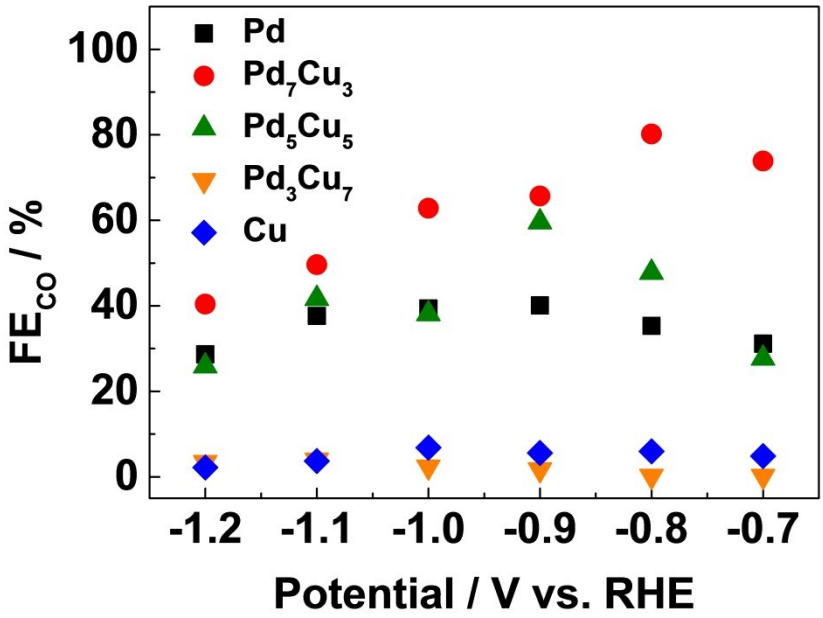

Fig. S1 Faradaic efficiencies for CO over the series of mesoporous paladium-copper bimetallic electrocatalysts for the electroreduction of CO_2.

Content:

$$\text{Faradaic efficiency (FE)} = znF / jt$$

where z (reaction electron number) = 2 for CO and H_2, n is the GC detected product molar number (mol cm^{-2}), F is the Faradaic constant (C mol^{-1}), j is the photocurrent (A cm^{-2}) and t is the reaction time (s).

Fig. S1 shows the electrochemical Faradaic efficiencies (FEs) for CO of the mesoporous Pd-Cu bimetallic alloys in the potential region from -0.7 V to -1.2 V vs. RHE. The corresponding FEs for H_2 at different applied potentials are summarized in Fig. S2. With alloying Pd with Cu gradually, the trends in FEs for CO and H_2 change obviously for all the mesoporous electrocatalysts. CO becomes to be the dominant product when the mesoporous bimetallic alloy contains more Pd than Cu. As the Cu ratio increases to a majority component, the FEs for CO deceases dramatically. The optimal ratio appears at Pd_7Cu_3, in which the highest FE for CO exceeds 80% at -0.8 V vs. RHE. Thus, the mesoporous Pd_7Cu_3 bimetallic alloy was selected as the cathode catalysts to construct the PEC device.

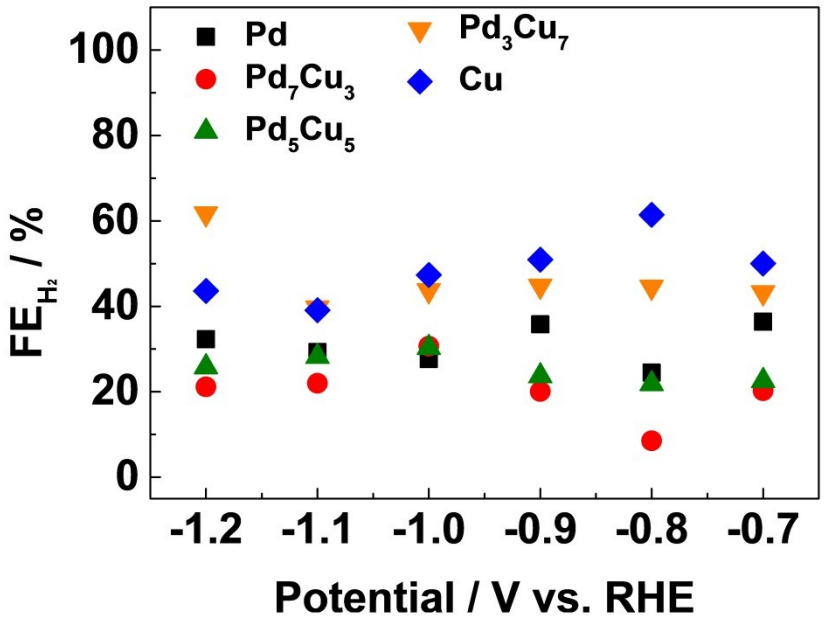

Fig. S2 Faradaic efficiencies for H_2 over the series of mesoporous paladium-copper bimetallic electrocatalysts for the electroreduction of CO_2.

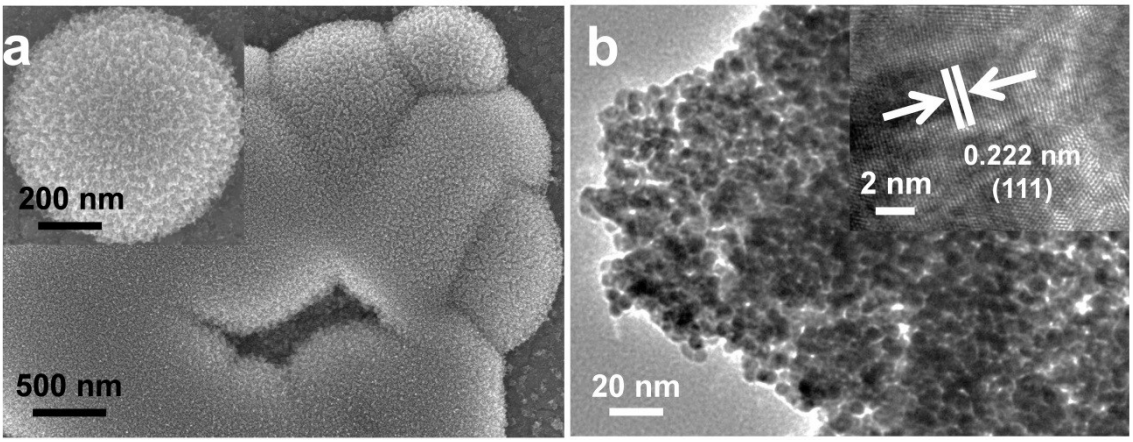

Fig. S3 a) Top-surface SEM image and b) TEM (HRTERM) image of mesoporous Pd_7Cu_3 alloy.

Content:

Fig. S3 shows the top-surface SEM and TEM images of the mesoporous Pd_7Cu_3 alloy. The surface exhibits a cauliflower-like structure with highly dispersed mesopores and uniform sizes. The HR-TEM image (Fig. S3b) shows a lattice fringes correspond to the crystal plane (111) (d = 2.22 Å), which is between the characteristics of face centered cubic Pd (d = 2.24 Å) and Cu (d = 2.09 Å) crystal phase in the (111) plane.

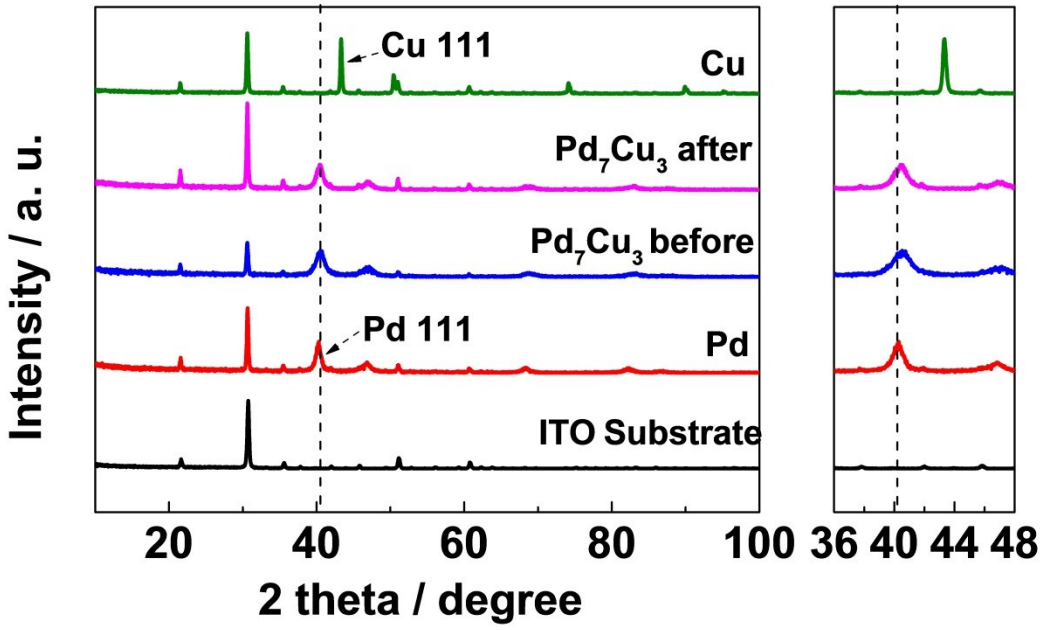

Fig. S4 XRD patterns of mesoporous Pd_7Cu_3 alloy before and after the PEC measurements.

Content:

The XRD patterns exhibit that the (111) peak of Pd_7Cu_3 can be observed between Pd (111) peak and Cu (111) peak (Space group: Fm-3m). It thus confirms the successful preparation of Pd-Cu bimetallic alloys. Moreover, it does not show any change after the PEC measurements (pink line).

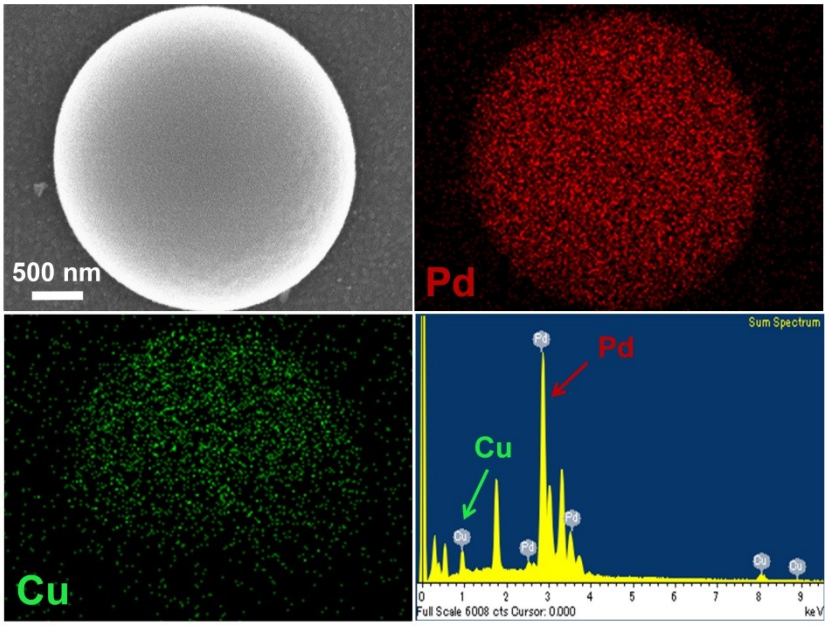

Fig. S5 EDX mapping of mesoporous Pd_7Cu_3 alloy.

Content:

The EDX mapping analysis confirms that Pd and Cu are homogeneously distributed within the mesoporous alloys. The ratio of Pd_7Cu_3 from EDX analysis is 92.63 : 7.37 (Weight%) and 88.25 : 11.75 (Atomic%). Since our prepared Pd-Cu alloy is a very thin film, the EDX analysis cannot provide accurate stoichiometric compositions of Pd and Cu within the alloys. ICP-OES measurements were carried out for the elemental analysis as shown in our previous report.[1] The content of both palladium and copper in the products linearly varied with the corresponding metallic precursors and accorded well with the stoichiometric ratios in the starting electrolyte solutions for sample preparation.

1. M. Li, J. Wang, P. Li, K. Chang, C. Li, T. Wang, B. Jiang, H. Zhang, H. Liu, Y. Yamauchi, N. Umezawa and J. Ye, J. Mater. Chem. A, 2016, 4, 4776-4782.

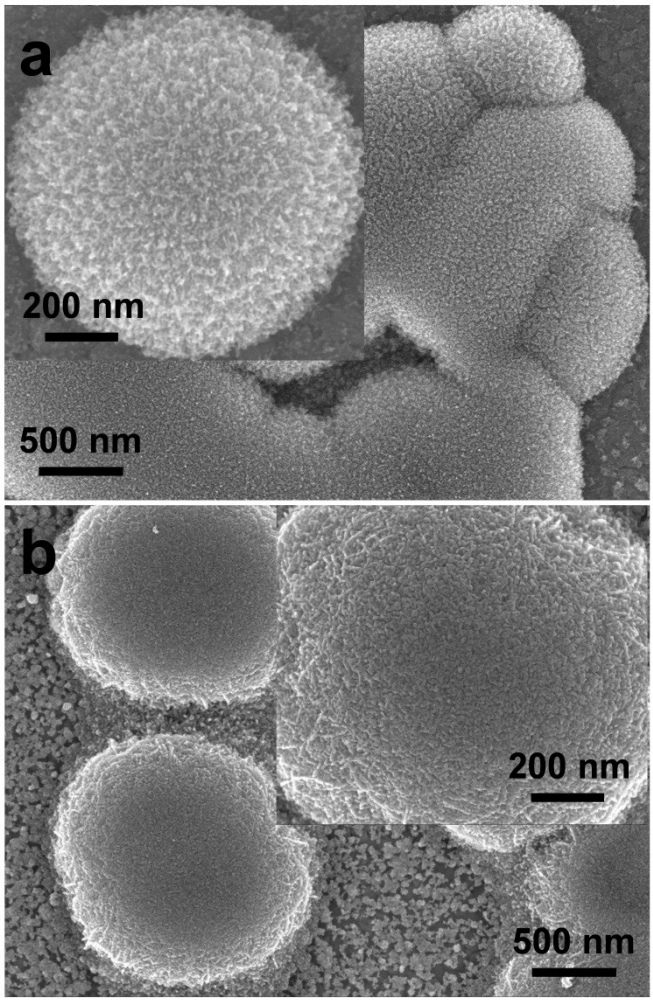

Fig. S6 Top-surface SEM images of a) mesoporous and b) nanoparticle Pd_7Cu_3 alloys.

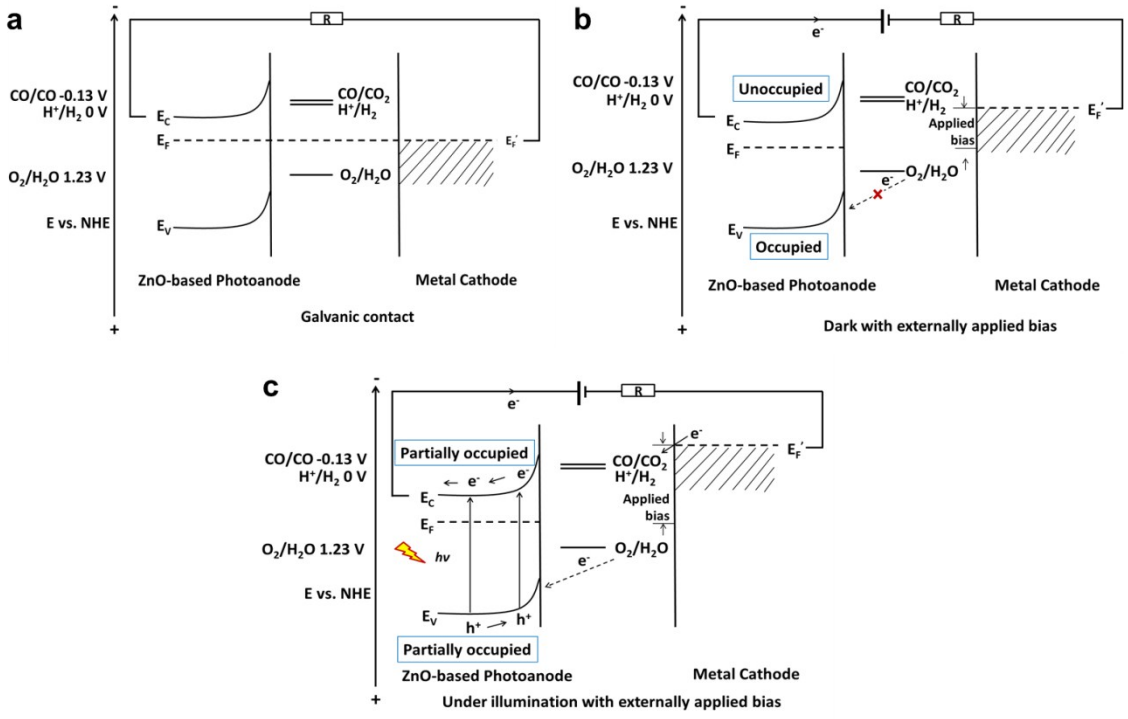

Fig. S7 Band diagram of PEC components a) after galvanic contact between the ZnO-based photoanode and Pd-Cu alloy metal cathode, b) with externally applied bias in the dark and c) under illumination and with externally applied bias.

Content:

After galvanic contact (Fig. S7a), the Fermi levels equilibrate with each other. When applying external bias (cathode negative and photoanode positive) in the dark (Fig. S7b), the Fermi level (EF') of metal cathode shifts to negative potentials and the Fermi level (EF) of ZnO-based photoanode shifts to positive potentials. In this case, the valence band of ZnO is fully occupied in the dark and the electrons cannot transfer from water to the valence band of ZnO, thus water is oxidized by the conductive substrate of ZnO since our prepared ZnO is not a compact film. However, the electrons in VB receive the energy of photons and can be excited to the CB under illumination (Fig. S7c). Thus, the electrons can transfer from water to the VB of ZnO and water can be oxidized by the photogenerated holes at the VB of ZnO. On the other hand, the photogenerated electrons can be transferred to the metal cathode. When the Fermi level (EF') of metal cathode fully exceeding the thermodynamic reduction potentials CO/CO_2, the photocurrent increases with the applied bias. Due to the photogenerated electron-hole pair, the needed externally applied bias under illumination is smaller than that needed in dark to drive the redox reactions. Thus, it exhibits obvious dark and light performances.

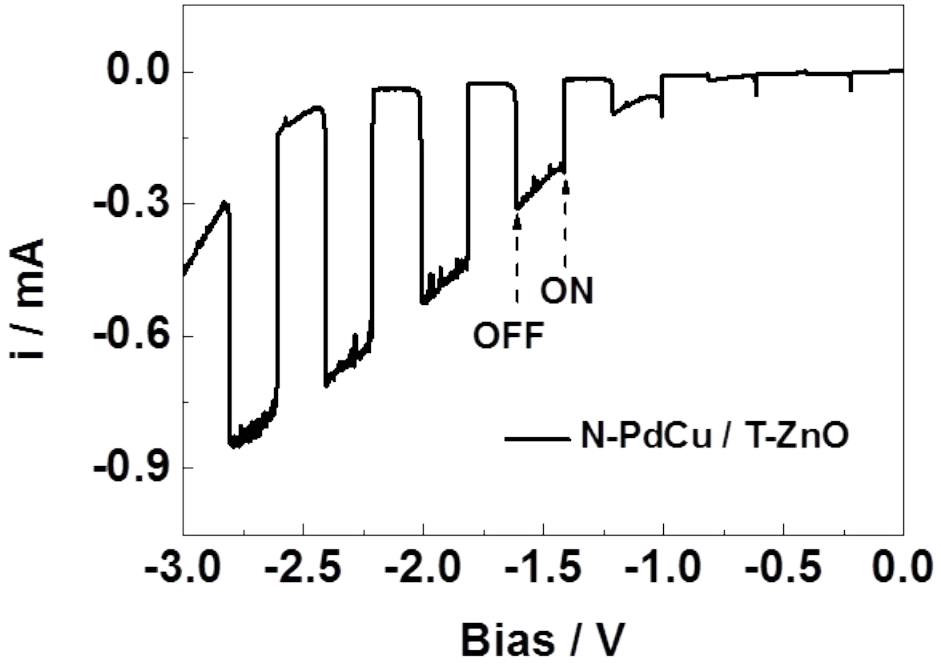

Fig. S8 Current-voltage curves over nanoparticle Pd_7Cu_3 (N-PdCu) alloy cathode and ternary CNTs-ZnO-Co_3O_4 NWs composite (T-ZnO) photoanode under chopped light illumination in a two-electrode cell.

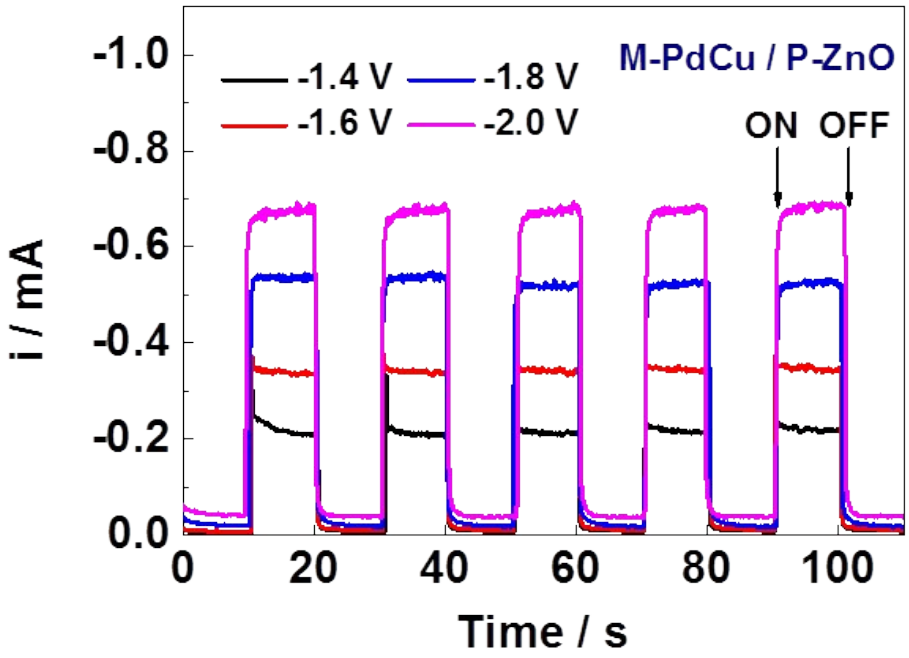

Fig. S9 Amperometric I-t curves of the PEC device over mesoporous Pd_7Cu_3 (M-PdCu) alloy cathode and pristine ZnO NWs (P-ZnO) photoanodes in a two-electrode cell at different applied biases.

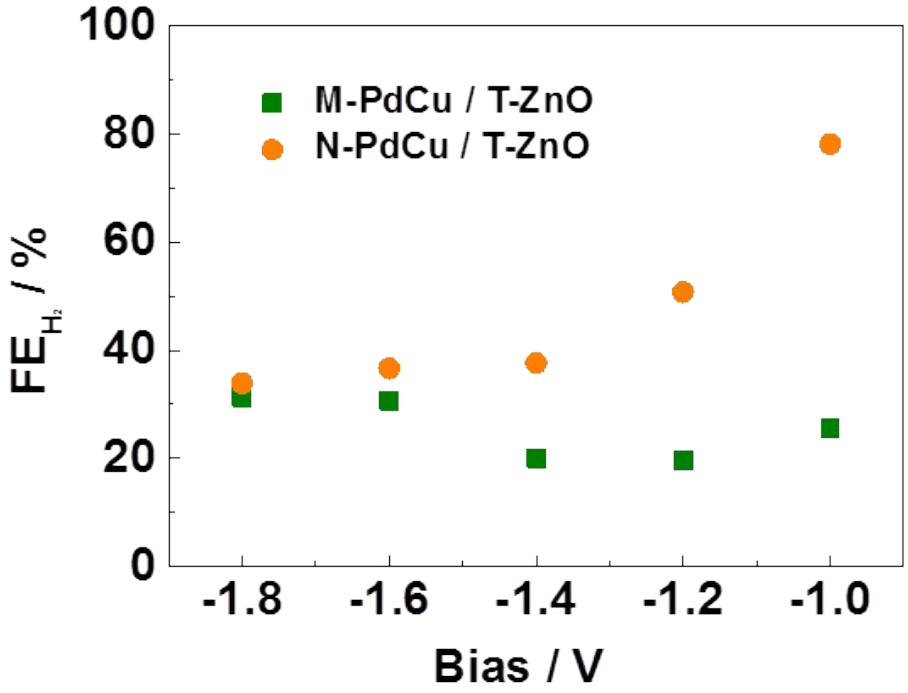

Fig. S10 Amperometric I-t curves of the PEC device over mesoporous Pd_7Cu_3 (M-PdCu) alloy cathode and pristine ZnO NWs (P-ZnO) photoanodes in a two-electrode cell at different applied biases

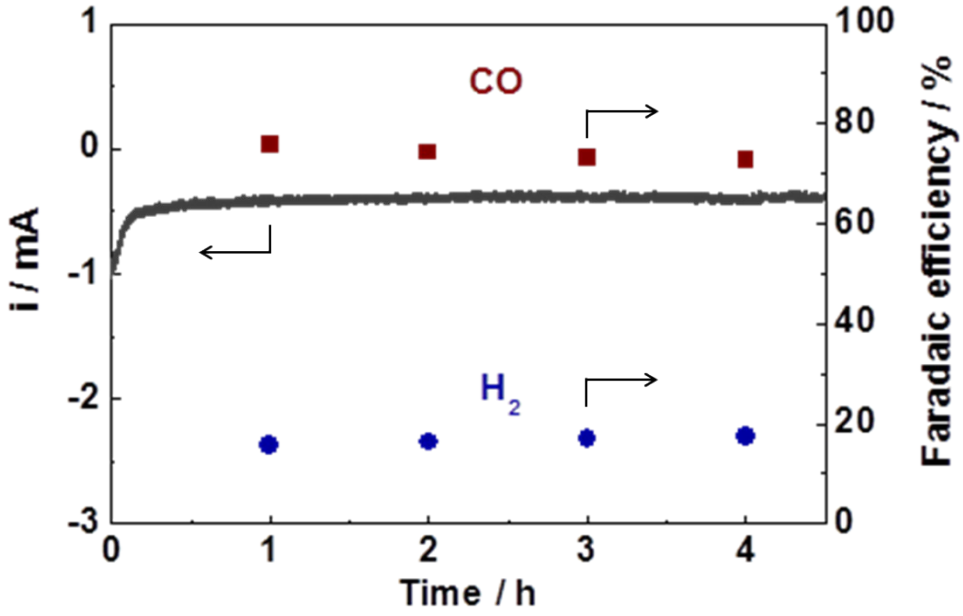

Fig. S11 Durability text over M-PdCu/T-ZnO (mesoporous Pd_7Cu_3 alloy cathode and ternary CNTs-ZnO-Co_3O_4 NWs composite photoanodes) at -1.2 V.

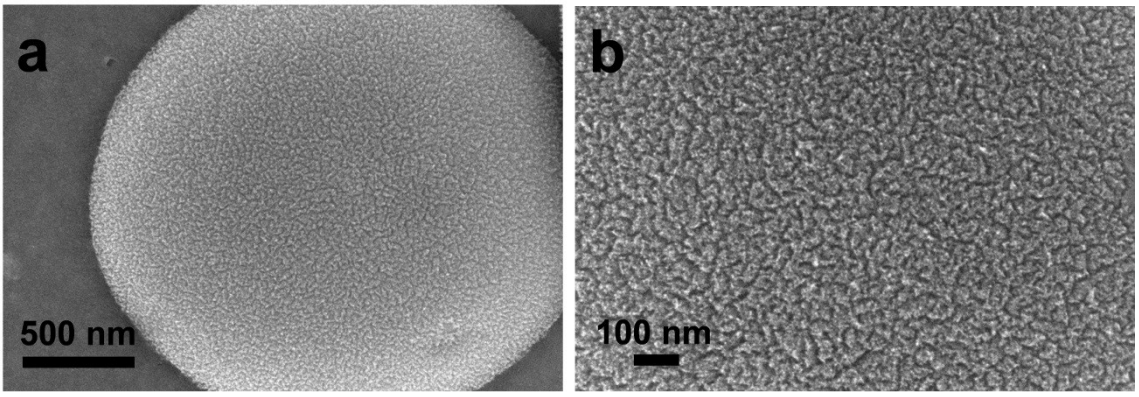

Fig. S12 a) and b) Top-surface SEM images of mesoporous Pd_7Cu_3 alloy after the PEC measurements.

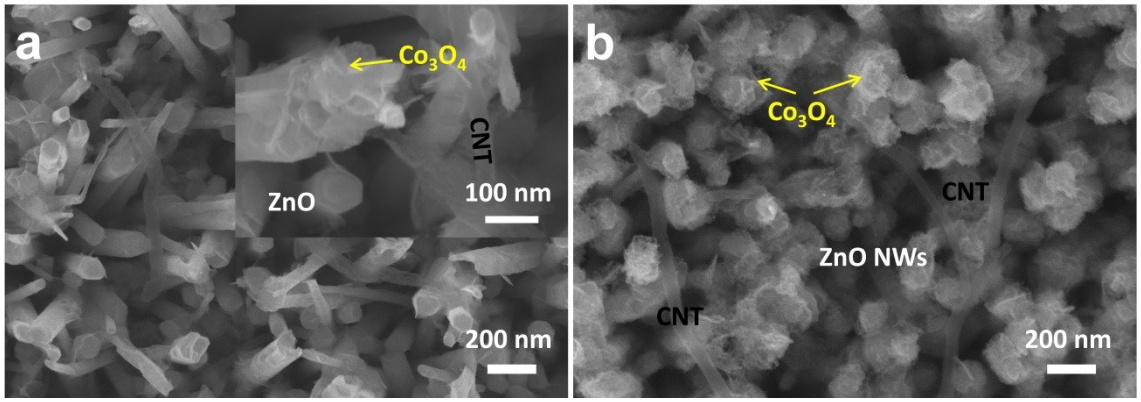

Fig. S13 SEM images of ternary CNTs-ZnO-Co_3O_4 NWs composite a) before and b) after the PEC measurements.

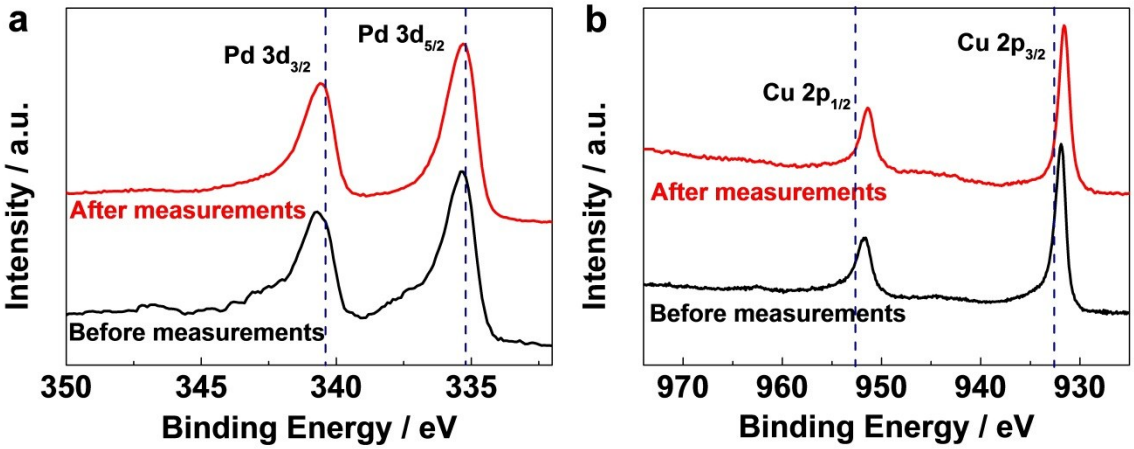

Fig. S14 XPS spectra of mesoporous Pd_7Cu_3 alloy a) before and b) after the PEC measurements.

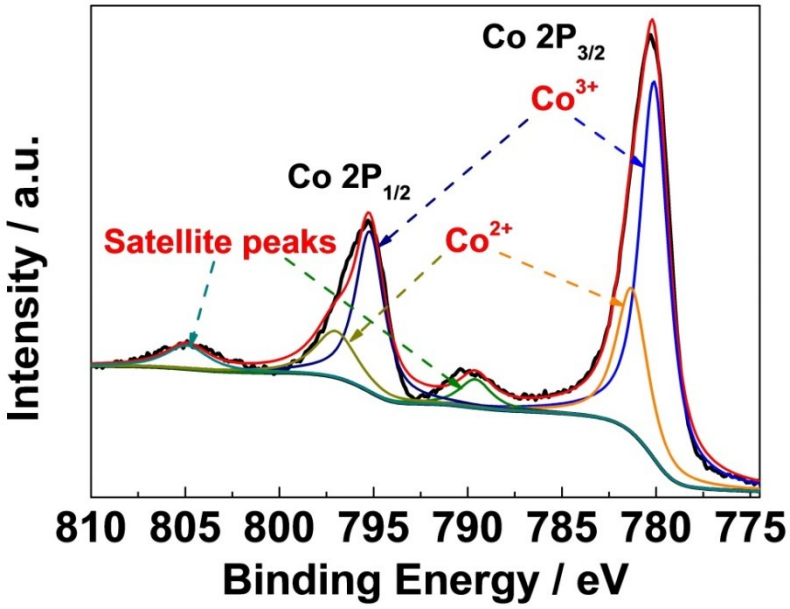

Fig. S15 XPS spectra of Co 2p for ternary CNTs-ZnO-Co_3O_4 NWs composite after the PEC measurements.

Content:

The two main Co 2p can also be decomposed to Co^{3+} and Co^{2+} oxidation state after the PEC measurements, which associated with the typical assignment of cobalt oxidation states in Co_3O_4. Besides, the satellite peak at ca. 790 eV is about 9 eV higher than the position of the main peak of Co 2p3/2, which also contributes the maintenance of Co_3O_4 after the PEC measurements.

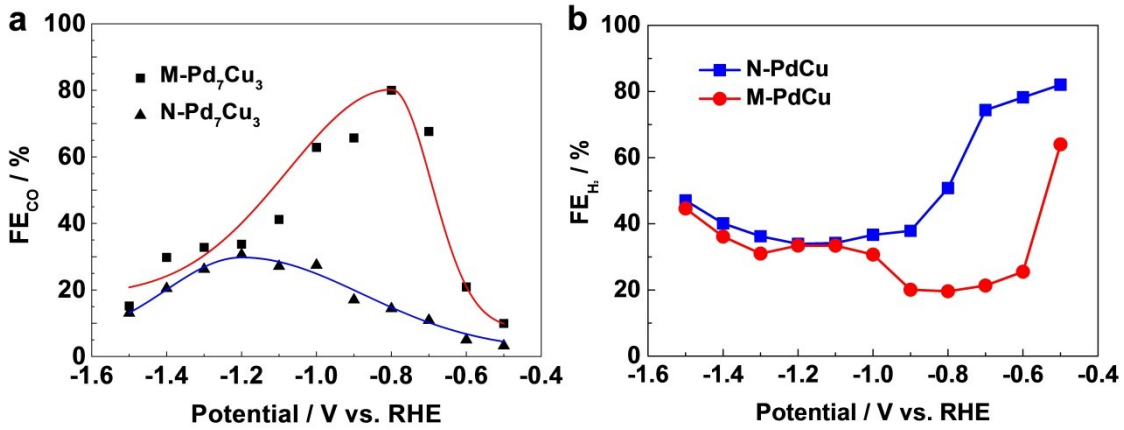

Fig. S16 Faradaic efficiencies for a) CO and b) H_2 of the electrochemical CO_2 reduction over mesoporous Pd_7Cu_3 (M-PdCu) and nanoparticle Pd_7Cu_3 (N-PdCu) alloys, with Pt and Ag/AgCl (in saturated KCl) electrode as counter and reference in a three-electrode cell system.

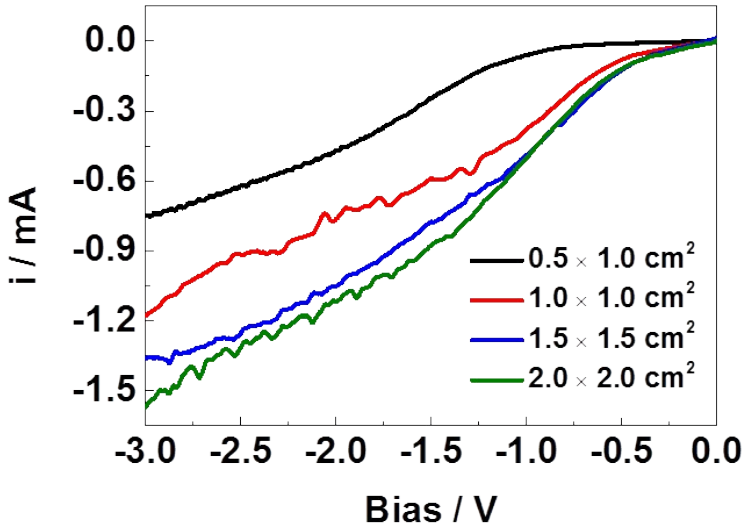

Fig. 17 Photocurrent responses of the assembly of fixed area mesoporous Pd_7Cu_3 alloy (M-PdCu) cathode (ca. 0.07 cm^2) and various areas of ternary CNTs-ZnO-Co_3O_4 NWs photoanode (T-ZnO).

Content:

The photocurrent responses of different area ratios between metal cathode and ZnO-based photoanode were examined. The M-PdCu alloy cathodes were prepared on purchased glassy carbon (GC) substrate (diameter = 3 mm, BAS Inc.) and thus the cathodic area was fixed as ca. 0.07 cm^2. The T-ZnO photoanodes were prepared on FTO substrate by a hydrothermal process. The T-ZnO photoanodes were prepared to 0.5 cm × 1.0 cm, 1.0 cm × 1.0 cm, 1.5 cm × 1.5 cm and 2.0 cm × 2.0 cm by cutting the FTO substrates to appropriate sizes. The photocurrent response increases and becomes approximate to each other with increasing the photoanode area. These results suggest that the overall photocurrent response is mainly controlled by the photoanodic side at the applied bias region. The photocurrent differences between the adjacent photoanode areas become smaller and smaller. Due to the size limit of our autoclave for hydrothermal preparation, we did not examine the photocurrent response on larger area photoanode. It can be deduced that if the photanode area can be larger to some extent, the photocurrent will not be increased with the area and the overall PEC reaction will be mainly determined by the cathodic side. Thus, in the point of realizing a maximum performance of our assembly of M-PdCu / T-ZnO, the area ratio between T-ZnO photoanode and M-PdCu cathode should be larger enough, so that the photoanode could support enough photogenerated electrons to the cathode. Because the FE of overall PEC reaction is mainly determined by the catalytic characteristic of the cathode materials, the maximum FE for CO will not be changed by enlarging the photoanode area. However, the optimal FE_{CO} can be obtained at more positive bias. For example, the maximum FE_{CO} (ca. 75%) was obtained at -1.2 V when the photoanode area is 1.0 cm × 1.0 cm. After enlarging the photoanode area to 2.0 cm × 2.0 cm, an identical FE_{CO} can be obtained at ca. -1.0 V.

Table S1. Total Faradaic efficiencies (FE) of CO and H_2 for the assembly of M-PdCu / T-ZnO.

Bias / V	FE_{CO}	FE_{H2}	FE_{Total}
-1.8	50.23	31.26	81.49
-1.6	62.83	30.69	93.52
-1.4	65.69	20.07	85.76
-1.2	74.68	19.42	94.10
-1.0	40.23	25.52	65.75

Content:

The summary of total Faradaic efficiencies of the two main products CO and H_2 was added in Table S1. The total FEs are higher than 80% at almost every applied bias. The other part can be assumed as the efficiency lost caused by the ohmic resistances of the external and internal circuits of the PEC, including: (1) electrodes, (2) electrolyte, (3) electrical leads (wires), (4) electrical connections and (5) measuring and control equipment.[2] In particular, the ohmic resistance of semiconductor is much larger than metal anode (Pt: ~ 0.14 Ω; ZnO: ~ 70 kΩ; measured by multimeter). Moreover, the connection resistance between ZnO and metal wire (Schottky contact) is also several orders of magnitude larger than that of metal/metal connection.[3] On the other hand, there should also be some other products, such as some trace amount of HCOOH (or $HCOO^-$) and other liquid phase products. In our current experimental system, the characterization has not been set up ready for the trace amount of liquid products. And these products are also assumed to contribute to some efficiency lost.

When comparing the PEC CO_2 conversion process (M-PdCu/T-ZnO, FE_{CO} ≈ 75%) with the electrochemical counterpart (M-PdCu/Pt FE_{CO} ≈ 80%), the FE_{CO} shows a slightly shrink. The shrink of FE_{CO} can be assumed as the efficiency lost caused by the ohmic resistances. On the other hand, the FE_{CO} of the electrochemical counterpart was measured by three-electrode cell, which can finely control the potential on Pd-Cu alloy electrode vs. NHE. The PEC process was measured by two-electrode, in which the applied bias is the bias gap between cathode and anode. The real reaction potentials vs. NHE on both anodic and cathodic side nonlinearly vary with the applied bias.[4] Thus, the FE_{CO} shrink may also be caused by the real potential differences on Pd-Cu vs. NHE.

2. T. Bak, J. Nowotny, M. Rekas and C. C. Sorrell, Int. J. Hydrogen Energy, 2002, 27, 991-1022.

3. C. Jagadish and S. J. Pearton, Zinc Oxide Bulk, Thin Films and Nanostructures: Processing, Properties, and Applications, Elsevier Science, 2011.

4. Z. Chen, H. Dinh and E. Miller, Photoelectrochemical Water Splitting: Standards, Experimental Methods, and Protocols, Springer New York, 2013.

Table S2. Comparison with the previous results of PEC CO_2 reduction to CO in aqueous electrolyte.

Materials	Surface orientation	Electrolyte	Metal particles on surface or in solution	Potential / V	Faradic efficiency
p-Si[5] (1.1 eV)	(111)	0.1 M $KHCO_3$	Au	-0.74 vs. SCE	CO (62.2%)
p-InP[6] (1.3 eV)	(100)	0.1 M Na_2SO_4	None	-1.2 vs. SCE	CO (16.1%) HCOOH (4.6%) H_2 (70.7%)
p-GaP[7] (2.3 eV)	(100)	0.1 M $KHCO_3$	None	-0.9 vs. Ag/AgCl	CO (11.9%) HCOOH (56.2%) H_2 (2.3%)
p-CdTe[6] (1.4 eV)	(111)	0.1 M Na_2SO_4	None	-1.2 vs. SCE	CO (43.3%) HCOOH (5.4%) H_2 (45.1%)
M-PdCu* /T-ZnO	N/A	0.1 M $KHCO_3$	None	Bias -1.2 in two electrode cell	CO (75%) H_2 (19%)

5. K. Hirota, D. A. Tryk, K. Hashimoto, M. Okawa and A. Fujishima, Elsevier, Amsterdam, 1998.
6. C. Delacourt, P. L. Ridgway, J. B. Kerr and J. Newman, J. Electrochem. Soc., 2008, 155, B42-B49.
7. A. J. Morris, G. J. Meyer and E. Fujita, Acc. Chem. Res., 2009, 42, 1983-1994.

* This work.